SEISMIC WAVELET PHASE ESTIMATION BY l_1-NORM MINIMIZATION

GABRIEL R. GELPI[1,2], DANIEL O. PÉREZ[1,3] and DANILO R. VELIS[1]

[1] *Facultad de Ciencias Astronómicas y Geofísicas, Universidad Nacional de La Plata, and CONICET, La Plata, Argentina.*
gabrielrg@fcaglp.unlp.edu.ar, velis@fcaglp.unlp.edu.ar
[2] *YPF Tecnología S.A., Av. Del Petróleo s/n, Berisso, Argentina.*
dperez@fcaglp.unlp.edu.ar

(Received August 16, 2018; revised version accepted May 10, 2019)

ABSTRACT

Gelpi, G.R., Pérez, D.O. and Velis, D.R., 2019. Seismic wavelet phase estimation by l_1-norm minimization. *Journal of Seismic Exploration*, 28: 393-411.

A new method to estimate the phase of the wavelet when only seismic data is available is presented. Starting from the classical convolutional model of the seismic traces, the proposed technique is based in two hypotheses: (1) the wavelet phase can be adequately approximated by a constant; and (2) the series of reflection coefficients is non-Gaussian and/or sparse. Under these hypotheses, the deconvolution is viewed as an inverse problem regularized by the l_1-norm. The optimum wavelet phase is then obtained by selecting the constant phase rotation that leads to the deconvolved trace with minimum l_1-norm. We test the proposed method on synthetic and field data and we compare the results against those obtained by the classical method based on the Kurtosis maximization of the seismic data. The results show that the proposed technique is more accurate and reliable than the Kurtosis-based approach, especially when the effective data bandwidth is relatively poor and/or the non-Gaussianity hyphotesis is not fully satisfied.

KEY WORDS: l_1-norm, sparse-deconvolution, wavelet, phase, Kurtosis, FISTA.

0963-0651/19/$5.00

INTRODUCTION

Wavelet estimation is of paramount importance in the processing and interpretation of seismic data, including trace inversion, deconvolution, well tie and lithological analysis (Yilmaz, 2001; Lu, 2005; Herron, 2011; Yuan and Wang, 2011). While the estimation of the amplitude spectrum does not present major difficulties (Robinson and Treitel, 2002), the estimation of the wavelet phase is often a challenge when dealing with noisy data, poor effective data bandwidth and/or non-sparse reflectivity series.

Usually, the phase estimation problem is treated deterministically using the classical convolutional model and well log information (Herron, 2011; Ma et al., 2015). However, a statistical approach is required when well log data is not available in the area of study. In this sense, several authors have developed methods to estimate the wavelet phase directly from seismic data. Velis and Ulrych (1996), for example, followed the works of Tugnait (1987) and Lazear (1993) to estimate mixed phase wavelets using higher-order statistics. Similarly, methods based on the maximization of the Kurtosis (a fourth-order statistics) have been extensively studied by several authors (Longbottom et al., 1988; van der Bann, 2008; van der Bann and Fomel, 2009; Ma et al., 2015; Xu et al., 2012). Since the Kurtosis of a wavelet decreases as the phase diverges from zero, these methods look for the constant phase rotation that maximizes the kurtosis of the seismic trace. Kurtosis-based methods are robust in presence of noise and effective when the reflectivity is sparse. Contrarily, they are rather insensitive to changes in phase for data with narrow bandwidth or near-Gaussian reflectivities (Velis and Ulrych, 1996).

The method that we propose aims at overcoming the aforementioned difficulties. Unlike the Kurtosis-based methods that maximize the Kurtosis of the data, we minimize the l_1-norm of the deconvolved traces. In practice, we obtain the optimum phase by searching for the constant phase rotation that leads to deconvolved traces with minimum l_1-norm. By virtue of the sparse deconvolution process, the method allows us to estimate the phase of the seismic wavelet directly from the seismic data even when the effective data bandwidth and the reflectivity sparseness are relatively poor. One may argue that the two key hypothesis, sparseness and constant-phase, may impose strong limitations on the applicability of the technique. However, sparseness is an hypothesis that has been effectively used to solve the seismic deconvolution problem by various authors (Taylor et al., 1979; Oldenburg et al., 1983; Sacchi, 1997; Velis, 2008; Pérez et al., 2013, 2017, e.g.). Although the real subsoil structure is rather continuous than sparse, it is well-known that actual reflectivity coefficients derived from well-log data follow a non-Gaussian distribution (Walden and Hosken, 1986; Velis, 2003). Regarding the wavelet phase, it is also well-known that it can be simpler than we think, as shown by Neidell (1991). Indeed, the constant-phase assumption has been successfully used for many applications, including

well-to-seismic ties, deconvolution and zero-phasing seismic data (Levy and Oldenburg, 1987; White, 1988; Neidell, 1991; van der Bann, 2008; Edgar and van der Bann, 2011; Wang et al., 2014, e.g.).

The paper is organized as follows. First, we explain the proposed wavelet phase estimation method, define all relevant equations and parameters, and provide a step-by-step description of the algorithm. Second, we test the method using synthetic and field data examples comparing the performance of the l_1-norm technique against the classical Kurtosis-based approach. In addition, we carry out a sensitivity analysis to assess the impact of various data conditions on the effectiveness of their results. Finally, we summarize the main conclusions.

THEORY

Given a seismic section **S** composed of n_t traces, we aim to obtain an estimation of the phase φ of the source wavelet **w**. To this end, we rely on three hypotheses: (1) the convolutional model is valid; (2) the wavelet phase φ can be adequately approximated by a constant value; and (3) the series of reflection coefficients **x** associated with each trace is non-Gaussian and/or sparse. As described in the Introduction, we assume that the optimum wavelet phase is the constant phase rotation that minimizes the l_1-norm of the sparse-spike deconvolved traces.

Given **w**, the sparse-spike deconvolution of **S** is carried out, trace by trace, by minimizing

$$J(\mathbf{x}) = \| \mathbf{W}\mathbf{x} - \mathbf{s} \|_2^2 + \lambda \| \mathbf{x} \|_1, \tag{1}$$

where s is the seismic trace, x the reflectivity series and **W** the convolution matrix associated with **w**. The cost function $J(\mathbf{x})$ is composed of two terms that impose different constraints on x. The first term represents the misfit between the modeled and the observed data. Its minimization ensures that the estimated solution honors the observed data within a given tolerance. The second term represents the regularization term. Its minimization promotes sparse-spike solutions. The overall impact of the regularization is controlled by the trade-off parameter λ, which we must determine beforehand.

For the sake of simplicity, in this work we explore the space of the phase values using a grid search procedure, although more efficient alternatives like gradient-based methods can be used. In each step of the grid search the rotated wavelet is given by

$$\mathbf{w}^{rot} = cos(\phi)\mathbf{w}^0 + sin(\phi)HT\{\mathbf{w}^0\}, \tag{2}$$

where φ is the constant phase rotation, $\mathbf{w^0}$ is a zero phase wavelet and $HT\{\cdot\}$ is the Hilbert transform (Levy and Oldenburg, 1987; Robinson and Treitel, 2002). We obtain the zero phase wavelet by calculating the amplitude spectrum average over all available traces within a given time-offset window and performing the inverse Fourier transform. To improve the estimation, we apply a Hamming taper to smooth the average spectrum and to include some prior information about the wavelet length if it is available (van der Bann, 2008).

For each rotated wavelet, we carry out the sparse-spike deconvolution of each trace **s** by minimizing eq. (1). Then, and for the sake of robustness, we assign the mean value of all the l_1-norms of the estimated reflectivities to the corresponding phase rotation. Once the grid search procedure is completed, we choose the optimum phase rotation as the one that leads to the reflectivity with minimum mean l_1-norm. It is worth notice that rotations up to ±20◦ do not significantly modify the shape of the wavelet and it is not easily distinguished at a glance (Levy and Oldenburg, 1987). Therefore, solutions differing within that range are equally acceptable. Algorithm 1 details the aforementioned process.

Algorithm 1

input: Seismic section $\mathbf{S}$, trade-off parameter λ

output: Estimated phase $\hat{\phi}$

1: Estimate a zero phase wavelet $\mathbf{w}^0$.

2: Select m test angles ϕ_k: $\phi_{min} < \phi_k < \phi_{max}$

3: **for** $k = 1$ to m **do**

4: $\quad \mathbf{w}_k^{rot} = cos(\phi_k)\mathbf{w}^0 + sin(\phi_k)HT\{\mathbf{w}^0\}$

5: $\quad$ **for** $i = 1$ to n_t **do**

6: $\quad\quad \hat{\mathbf{x}}_i = \underset{\mathbf{x}}{\operatorname{argmin}}\, J(\mathbf{x}; \mathbf{s}_i, \mathbf{w}_k^{rot})$

7: $\quad$ **end for**

8: $\quad f(\phi_k) = \frac{1}{n_t}\sum_{i=1}^{n_t} \| \hat{\mathbf{x}}_i \|_1$

9: **end for**

10: $\hat{\phi} = \underset{\phi_k}{\operatorname{argmin}}\, f(\phi_k),\ k = 1, .., m$

Step 6 in Algorithm 1 repeatedly requires the minimization of eq. (1). The field of study of the algorithms developed to efficiently perform this task is vast and is constantly growing. Just to give some examples we can name the algorithms IRLS (Beaton and Turkey, 1974), ISTA (Daubechies et al., 2004) or TwIST (Bioucas-Dias and Figueiredo, 2007). In this work we use the Fast Iterative Shrinkage-Thresholding Algorithm (FISTA) (Beck and Teboulle, 2009), as described in Pérez et al. (2013). FISTA is an extension of the classical gradient algorithm to solve large-scale linear inverse problems in a simple way. At each iteration only matrix-vector multiplications, and no matrix inversions, are required. In this context, FISTA provides sparse-spike solutions in a simple and effective way. Readers are referred to the cited article for a detailed description of the algorithm.

As for the trade-off parameter λ, it is worth to mention that it is not unique and may exist a range of λ values for which the corresponding solutions honor the observed seismic data equally well. Often, the selection of the trade-off parameter is based on personal judgments, especially when the data noise is unknown (Farquharson and Oldenburg, 2004). In this context, we will show that there is a range of λ values for which the minimum of the corresponding l_1-norm curves coincide, within a small tolerance error, with the actual phase.

NUMERICAL RESULTS

We consider 3 synthetic examples and one field data example. The first synthetic example aims at demonstrating that the selection of the trade-off parameter in eq. (1) is not critical. The second example shows a statistical sensitivity analysis of both the proposed and the Kurtosis-based methods to data bandwidth and reflectivity sparseness. In the third example we challenge both methods using data generated with a portion of the 2D Marmousi2 model (Martin et al., 2006). It is worth noting that in the first two examples, the amplitude spectrum of the seismic wavelet is estimated directly from the data, as explained in the Theory section. In the third synthetic example, the actual amplitude spectrum is used, instead. Finally, we applied and compared the two methods on field data considering overlapping windows in time to take into account wavelet non-stationarity.

Synthetic data examples

Example 1: Selecting the trade-off parameter

In this example we analyzed the behavior of the estimated phase rotations with respect to the elected trade-off parameter λ. The literature

reports various methods to select it (Farquharson and Oldenburg, 2004; Malinverno and Briggs, 2004; van den Berg and Friedlander, 2008; Hennenfent et al., 2008). In general, the selection depends on the noise level of the data at hand. It is worth notice that a reckless selection may lead to solutions that do not honor the observed data. Even so, in this numerical example we show that for the phase estimation a rigorous adjustment is not necessary, as there exists a wide range of λ for which the solutions are acceptable.

For the analysis we considered the noisy trace shown in Fig. 1b, which we generated by convolving a sparse reflectivity series (Figs. 1a) with a 30Hz Ricker wavelet rotated −30°. We then added band-limited Gaussian noise with σ = max(|s|)/5 (i.e. S/N = 5). For each phase in the range -90° to 90°, we deconvolved the trace using 6 different λ's in the range 0.005 to 0.1. Fig. 2 shows how the l_1-norm of the deconvolved trace varies with φ for the selected 6 different λ values. Despite the wide range of the trade-off parameter, we observe that the minima of all the curves are close to the expected φ value. This result suggests that the selection of λ is not critical for the correct estimation of the wavelet phase.

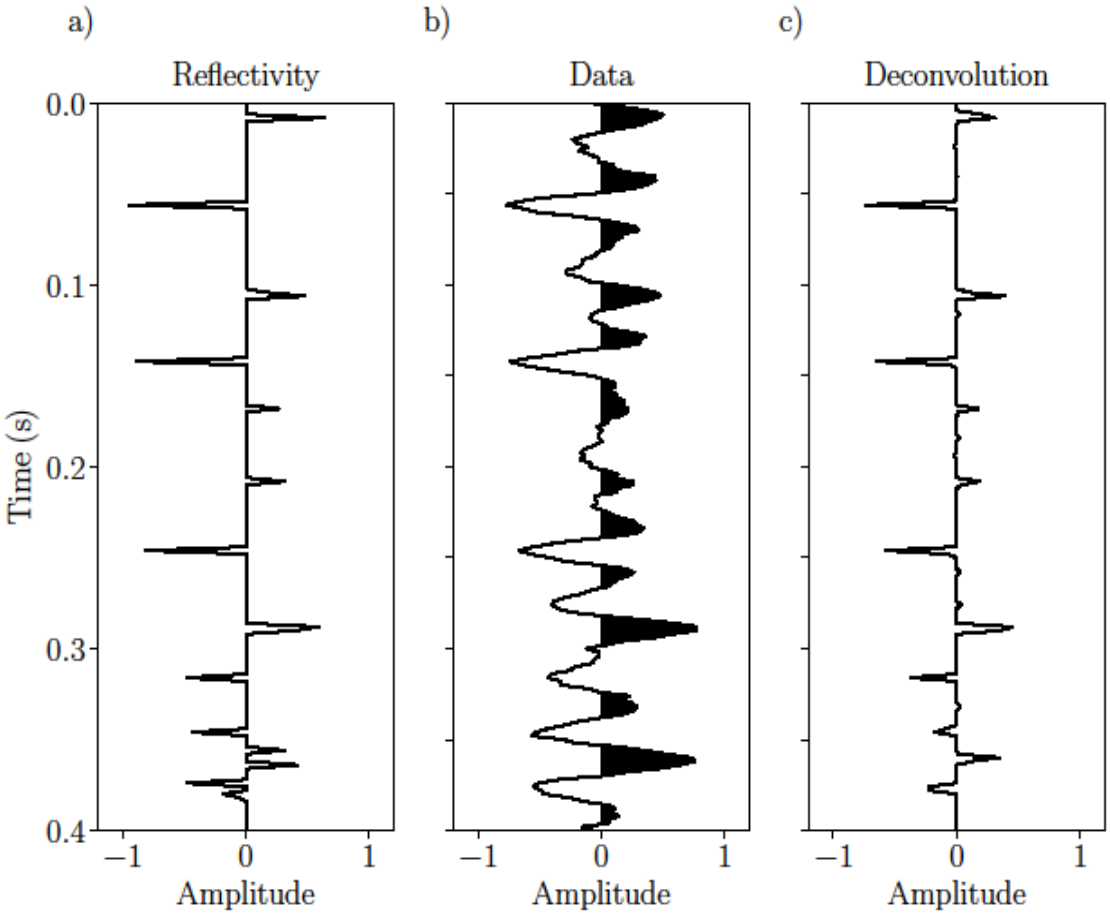

Fig. 1. Synthetic example 1: (a) reflectivity model, (b) noisy trace and (c) deconvoled trace using the wavelet phase estimated by the l_1-norm method.

The optimum phase rotation is finally obtained by selecting the one that leads to the minimum l_1-norm. The corresponding deconvolved trace is shown in Fig. 1c ($\lambda = 0.05$). As we can see, the estimated reflectivity clearly resembles the actual model, in spite of a visible underestimation of the spikes' amplitudes. This undesired effect is expected when leading with sparse solutions, as observed by several authors (Figueiredo et al., 2007; Gramfort et al., 2013, e.g.). A debiassing step might be used to properly compensate for this amplitude loss (Pérez et al., 2013).

Example 2: Sensitivity analysis

In this example we carried out a sensitivity analysis of the method to data bandwidth (BW) and reflectivity sparseness. To this end we generated sets of 1D noise-free synthetic data with different BW and sparseness. Reflectivities are Bernoulli-Gaussian models where the sparseness can be quantified by the percentage P of reflection coefficients identically non-zero. We considered values of P in the range 5 to 100% and wavelets with BW in the range 20 to 100 Hz, with steps of 2.5 for both variables. The wavelets were rotated 45°. Then, for each pair of values P and BW, we generated 100 realizations, where each realization consisted on generating a trace by convolving the rotated wavelet with a random reflectivity with the appropriate sparseness.

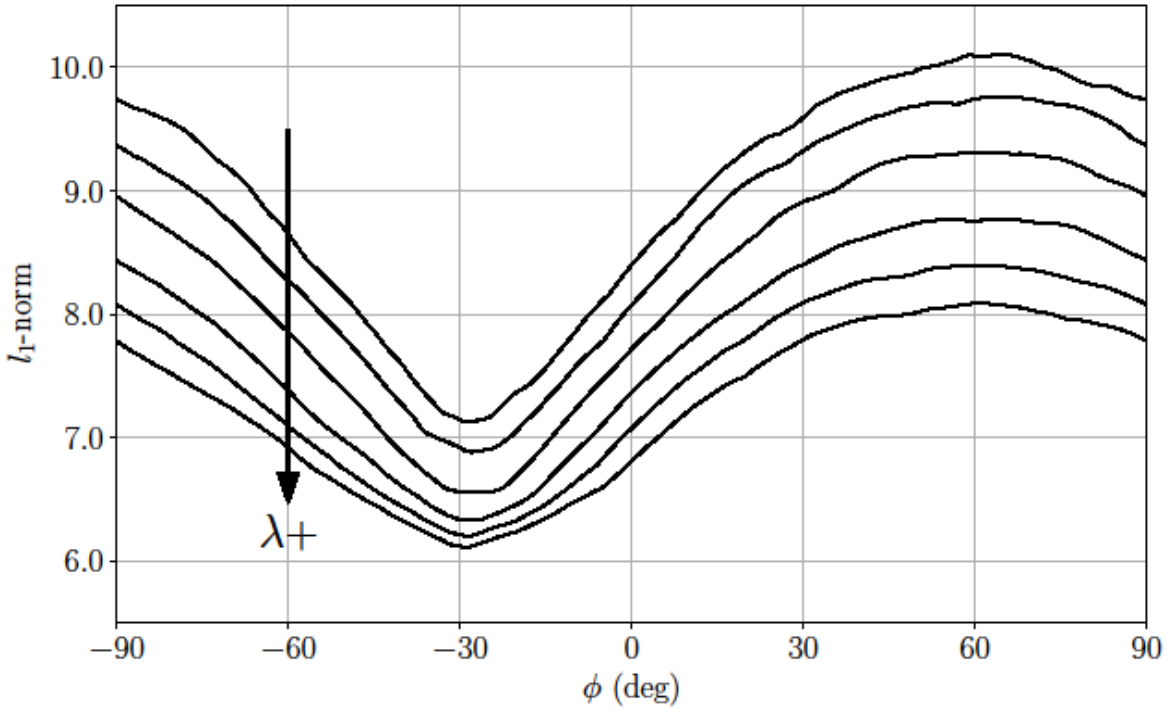

Fig. 2. Synthetic example 1: l_1-norm curves for $\lambda = 0.005$, 0.01, 0.025, 0.05, 0.075 and 0.1. The arrow denotes the direction of increasing λ.

To calculate the effectiveness of the method for any given BW and P pair, we estimated the phase from the corresponding 100 traces. Then, from those 100 solutions, we calculated the probability of estimating φ within a tolerance of ±20°. We carried out this procedure for all values of BW and P in the aforementioned ranges. For comparison purposes, we contrasted the estimated solutions with those obtained using the classical Kurtosis-based method. Contrarily to the well-known variance, a second-order statistics, Kurtosis is a fourth-order statistics that preserves phase information. It provides a measure for the "tailedness" of the distribution. Then, it can be interpreted as a measure of non-Gaussianity. The angle corresponding to the maximum kurtosis of the seismic trace determines the candidate wavelet phase, because in that case, each wavelet would become zero-phase and closer to a spike.

Fig. 3 shows the results of the sensitivity analysis. The first row shows the probability of estimating the correct phase within ±20°, using both the l_1-norm and the Kurtosis-based methods. The second and third rows show the estimated mean phases and their corresponding standard deviations, respectively. In general, we can see that the l_1-norm method is more robust than the Kurtosis-based method. In effect, the black region, where the probability of obtaining the correct phase within the given tolerance is high, is much larger for the l_1-norm method than for the Kurtosis-based method. As expected, the probability increases with BW but decreases with P in both cases. The second and third rows of Fig. 3 reinforce these conclusions, showing the advantages of the proposed method over the classical Kurtosis-based technique when data BW and sparseness are relatively poor. Note how mean values decrease significantly for large P and/or small BW. This is explained by the fact that in these situations, the distribution of the mean phase estimates becomes uniform in the search range (i.e., no phase information), which in this case is centered at zero degrees. On the other hand, the higher the BW and the sparseness, the closer the peak of the resulting distribution to the actual phase, as shown in Fig. 3, second row. For the sake of completeness, Fig. 4 shows the histograms of the 100 solutions corresponding to BW = 40 Hz, and P=5%, 10% and 20%. They show how the performance of both the l_1-norm and the Kurtosis-based methods decrease as the reflectivity models become less sparse, and vice-versa. Still, the l_1-norm method is more robust than the Kurtosis-based technique, consistently showing estimations closer to the actual phase.

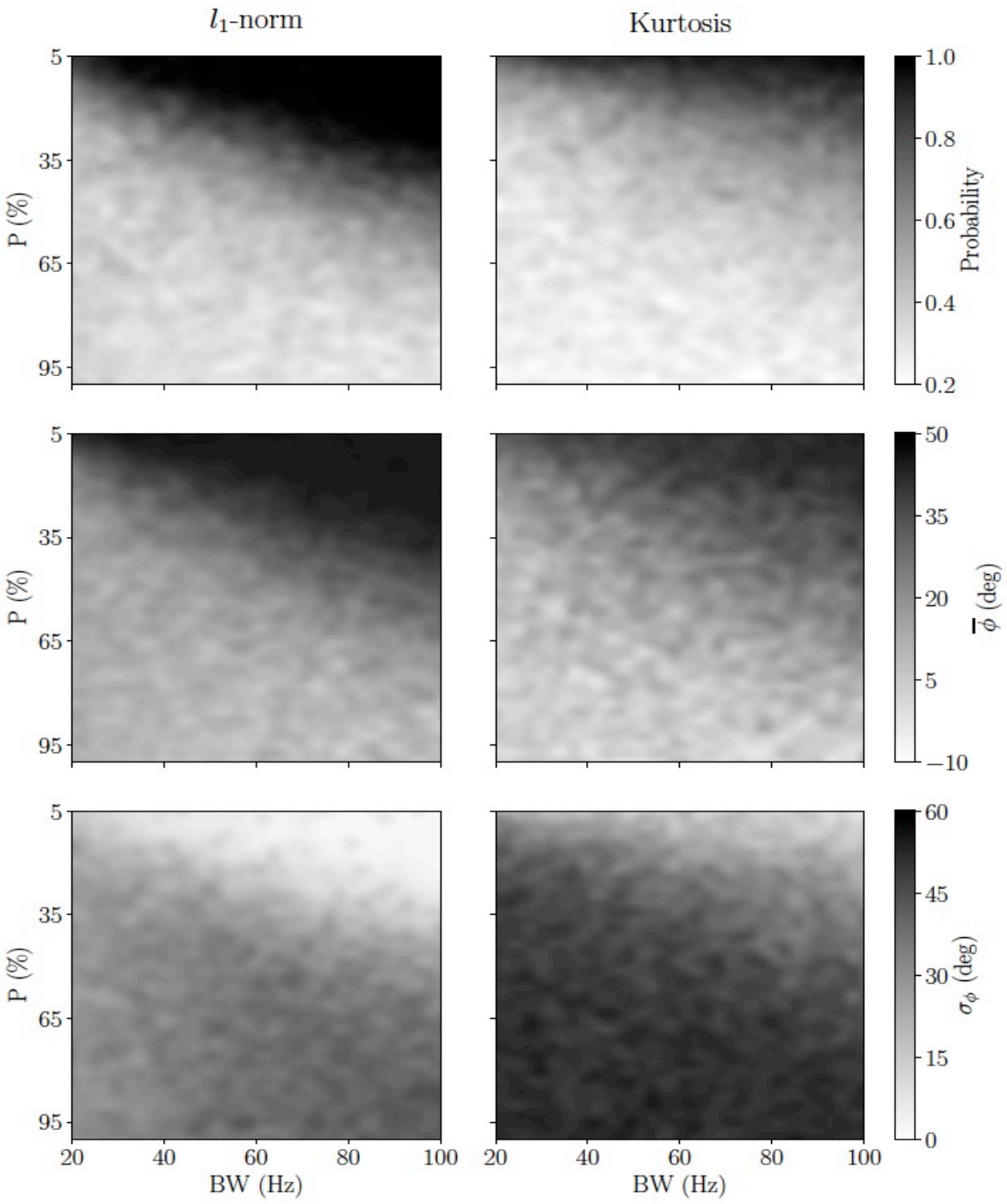

Fig. 3. Synthetic example 2. First row: Probability of encountering the correct phase within a tolerance of ±20° using the l_1-norm and Kurtosis-based methods. Second row: Estimated mean phases. Third row: Estimated phases standard deviations.

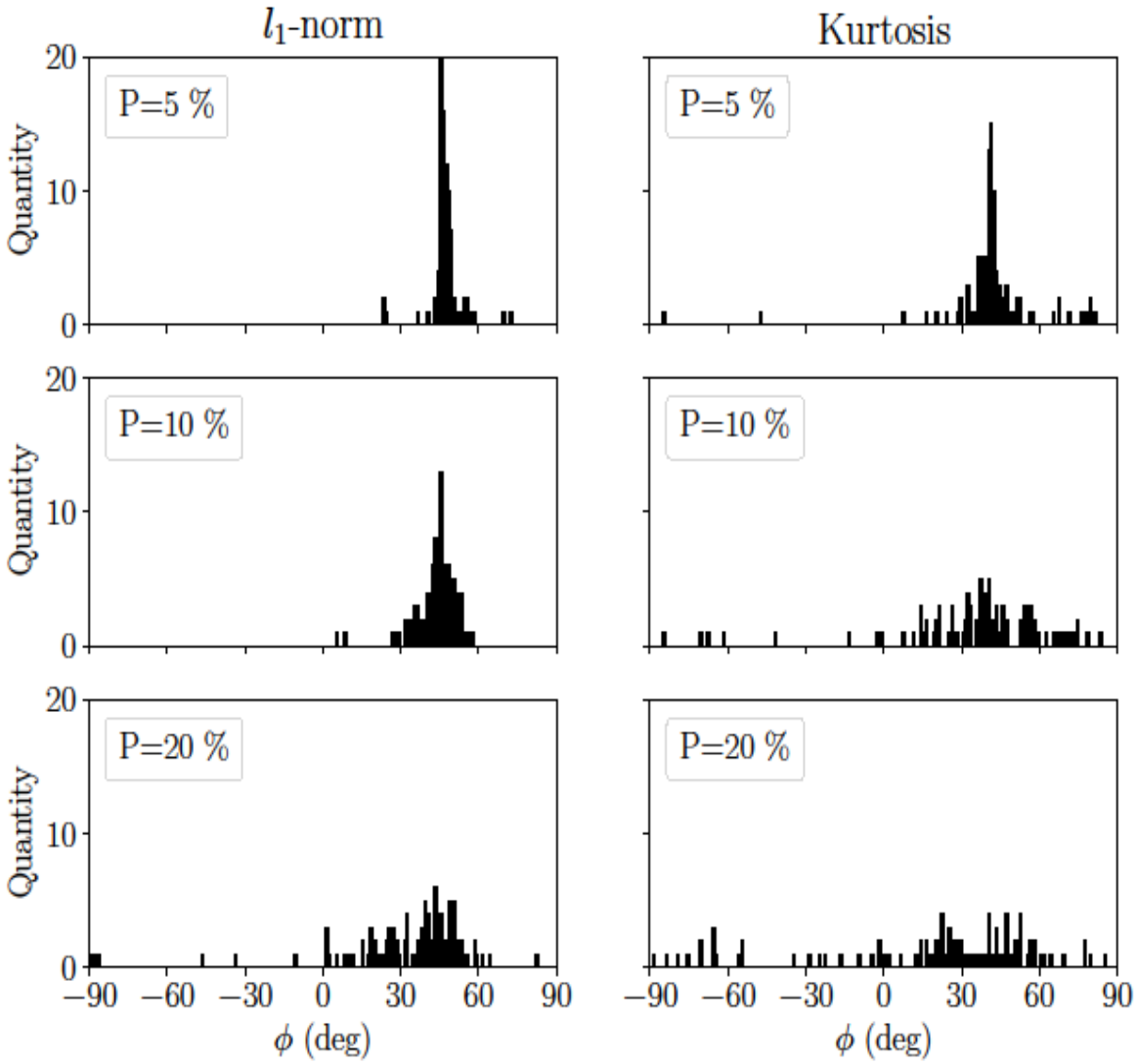

Fig. 4. Synthetic example 2: Histograms of the l_1-norm and Kurtosis estimations for BW = 40 Hz and various P.

Example 3: Test on the Marmousi2 model

In this example we tested the proposed method on 2D synthetic data and compared it against the Kurtosis-based approach. To generate the data we used a reflectivity that we extracted from the Marmousi2 elastic model (Martin et al., 2006), as shown in Fig. 5a. We generated noise-free seismic sections by convolving the reflectivity series with Ormsby-like wavelets spanning a BW range from 20 to 100 Hz, with a phase rotation of 30°. For statistical purposes, we generated 100 realizations by adding band-limited Gaussian noise. Figs. 5b and 5c show two sample sections where BW = 30Hz and 80 Hz, and S/N = 3. Contrarily to the previous two examples, in this test we did not estimate the amplitude spectrum from the data. Instead, we used the actual spectrum to avoid the errors associated with its estimation and focus the analysis on phase information only.

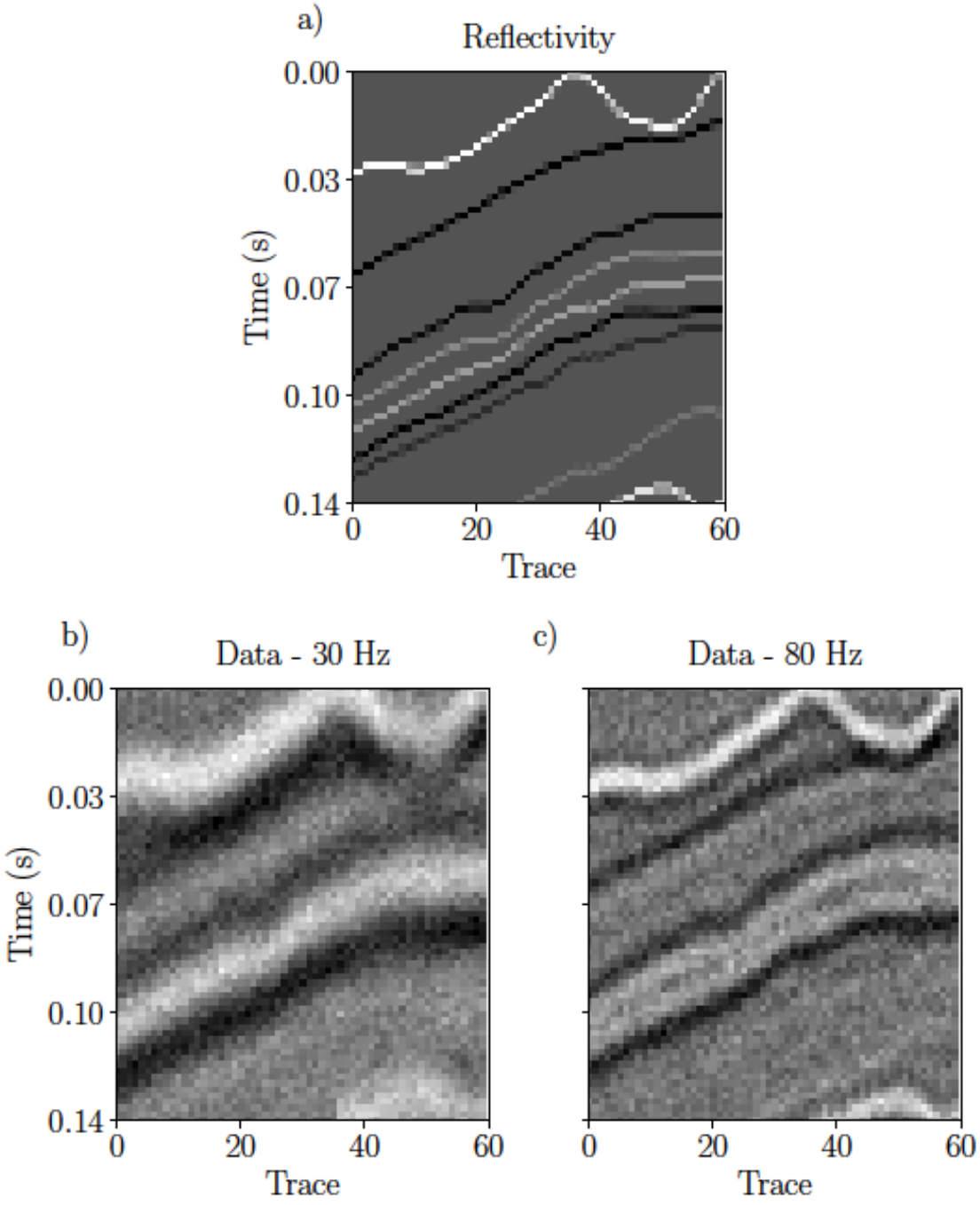

Fig. 5. Synthetic example 3: a) Reflectivity model extracted from Marmousi2, b) section with BW = 30 Hz, c) section BW = 80 Hz. In both cases, S/N = 3.

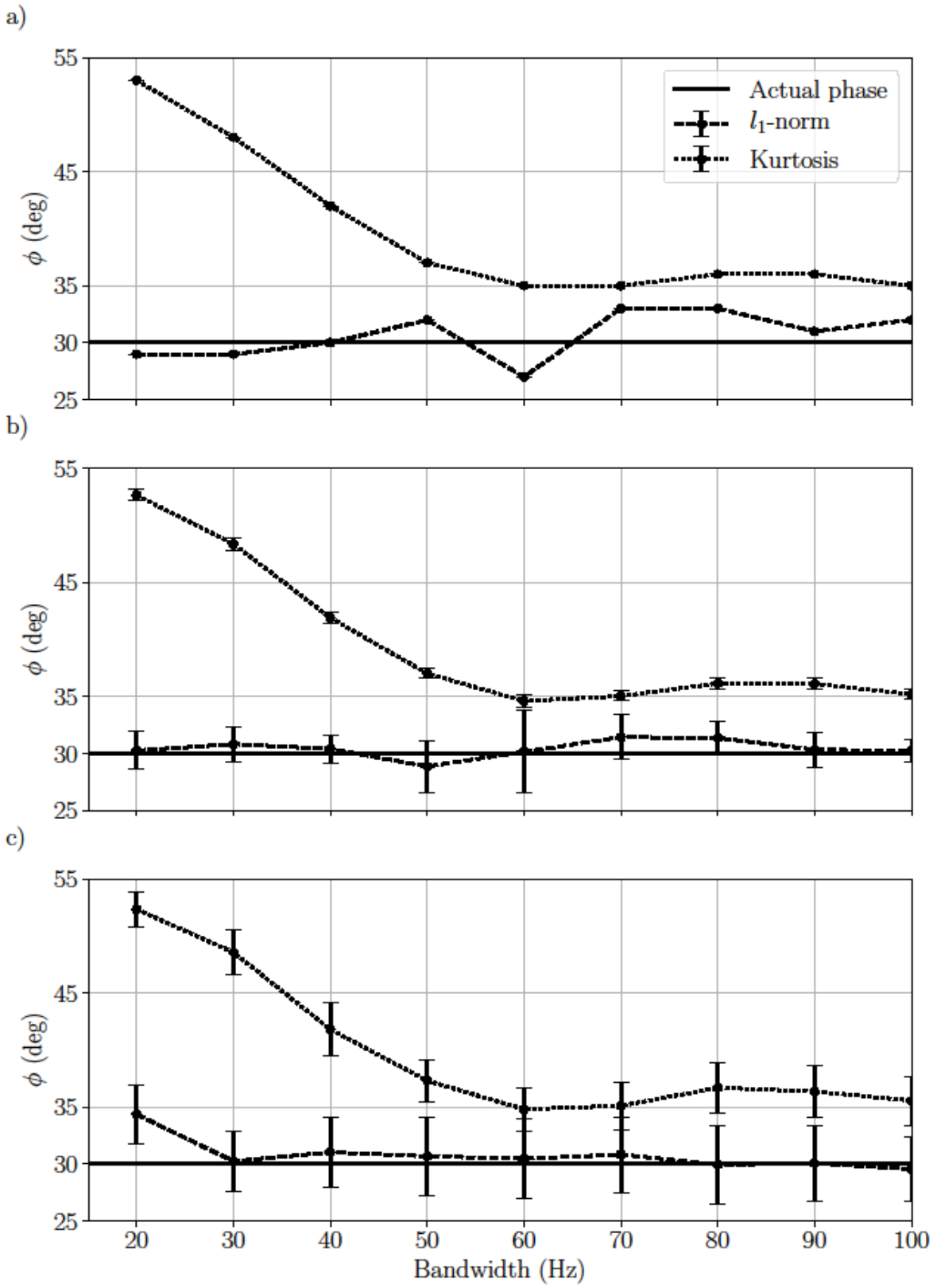

Fig. 6. Synthetic example 3. Performance of the l_1-norm and Kurtosis-based methods: (a) noise free data, (b) S/N = 15 and (c) S/N = 3.

The results are shown in Fig. 6. The first panel shows the estimated phases for the noise-free case. Although most solutions are in a range of ±20° around the actual phase for both methods, the l_1-norm approach was more accurate than the Kurtosis-based method for all the tested data BW's, being very accurate even for the lowest BW values. The second and third panels of Fig. 6 show the mean estimated phases, and their corresponding standard deviations, after the 100 realizations. As expected, the accuracy of the solutions improve for increasing BW and S/N ratio. Even so, in both cases the mean solutions estimated using l_1-norm method overcome those estimated using the Kurtosis-based approach, for all BW values. In contrast, the Kurtosis-based solutions show smaller standard deviations than the l_1-norm solutions. Thus, for a given BW and S/N, the Kurtosis-based technique is more robust than the l_1-norm method. On the other hand, its solutions are significantly biased, especially for the lowest BW values.

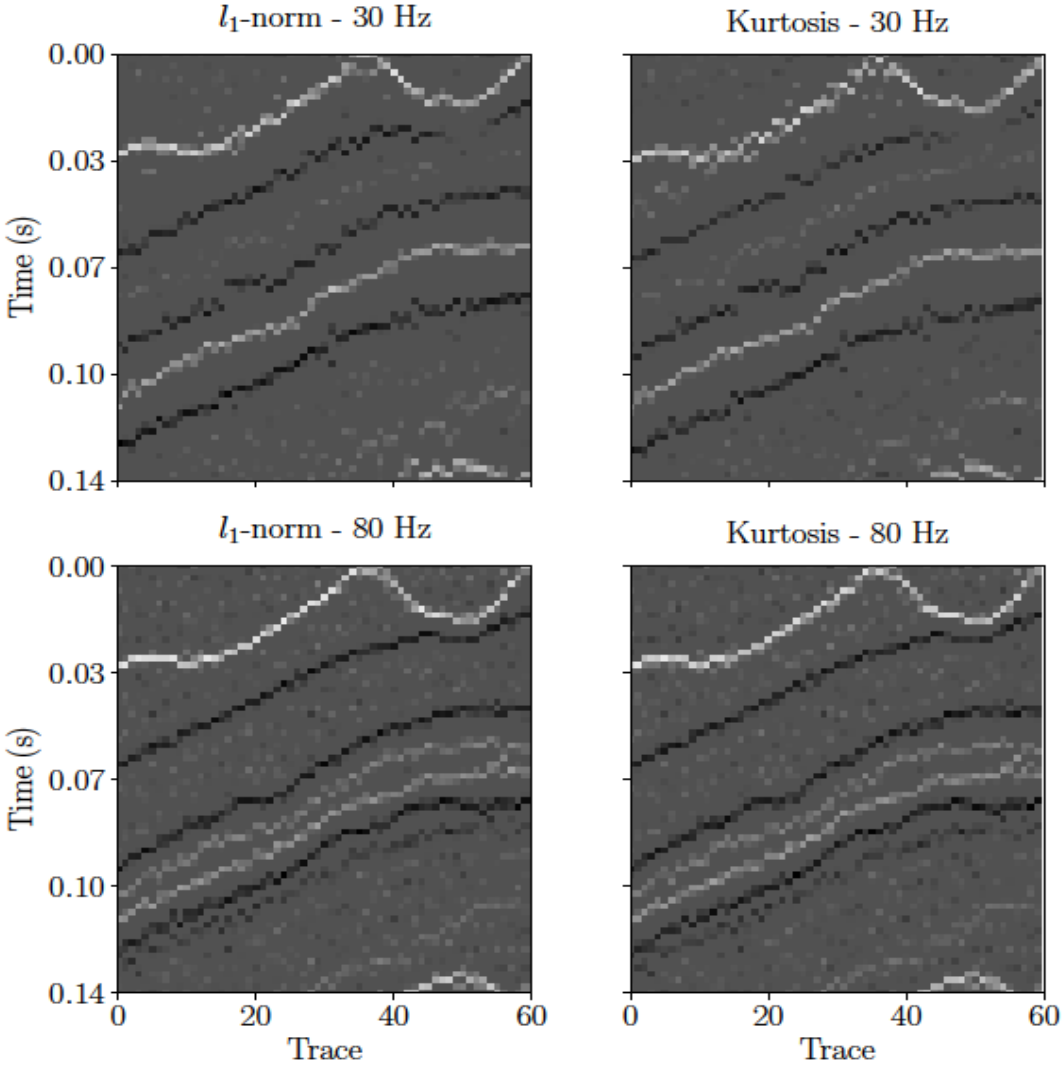

Fig. 7. Synthetic example 3: sparse-spike deconvolutions for the cases with BW = 30 Hz (first row) and 80 Hz (second row).

For illustrative purposes, Fig. 7 shows the corresponding sparse-spike deconvolutions of the data shown in Figs. 5b and 5c. In all cases the deconvolutions were carried out using $\lambda = 0.01$. A slight improvement is observed when using the l_1-norm phase over the Kurtosis-based one for the case with BW = 30 Hz. In the BW = 80 Hz case, the differences are negligible.

Field data example

The field section shown in Fig. 8a contains 200 traces, covering a time interval of 1.6 s with a sampling interval of 2 ms. To take into account the wavelet non-stationarity and possible phase changes throughout the section, we followed a strategy similar to that of van der Bann (2008). In this sense, we estimated individual wavelets for overlapping windows covering different ranges in time, and assigned the corresponding estimate to the center of the analysis window. For this example, we selected time windows of 0.8 s with an overlap of 0.4 s. This layout gave us a grid of 3 by 1 windows covering the whole dataset.

Figs. 9a and 9b show the estimated wavelets using the l_1-norm and the Kurtosis-based approaches, respectively. We observe that in the second and third time windows the estimates are similar, with phase differences below 25 degrees (see Table 1). Contrarily, the phase difference between the two estimates for the first window is close to 80 degrees. This discrepancy is reflected in the deconvolved sections shown in Figs. 8b and 8c, where the greatest differences are observed for the reflectors between 0.3 and 0.4 s. Figs. 8d and 8e show in detail the regions indicated with the white rectangles in Figs. 8b and 8c. These sparse-spike deconvolved sections were obtained after minimizing eq. (1) with $\lambda = 0.75$ and using the corresponding wavelets shown in Figs. 9a and 9b. For the sake of completeness, Fig. 10 shows the results for an isolated trace (trace #100). We can observe that the deconvolution using the wavelets estimated by means of the l_1-norm method (Fig. 10b) is more sparse and shows more well-defined reflectors than the deconvolution that relies on the wavelet estimates by means of the classical Kurtosis-based approach (Fig. 10c).

Table 1. Field data example: estimated phases for each overlapping window (in degrees).

Time window	l_1-norm	Kurtosis
1	-38	38
2	-83	-58
3	-53	-76

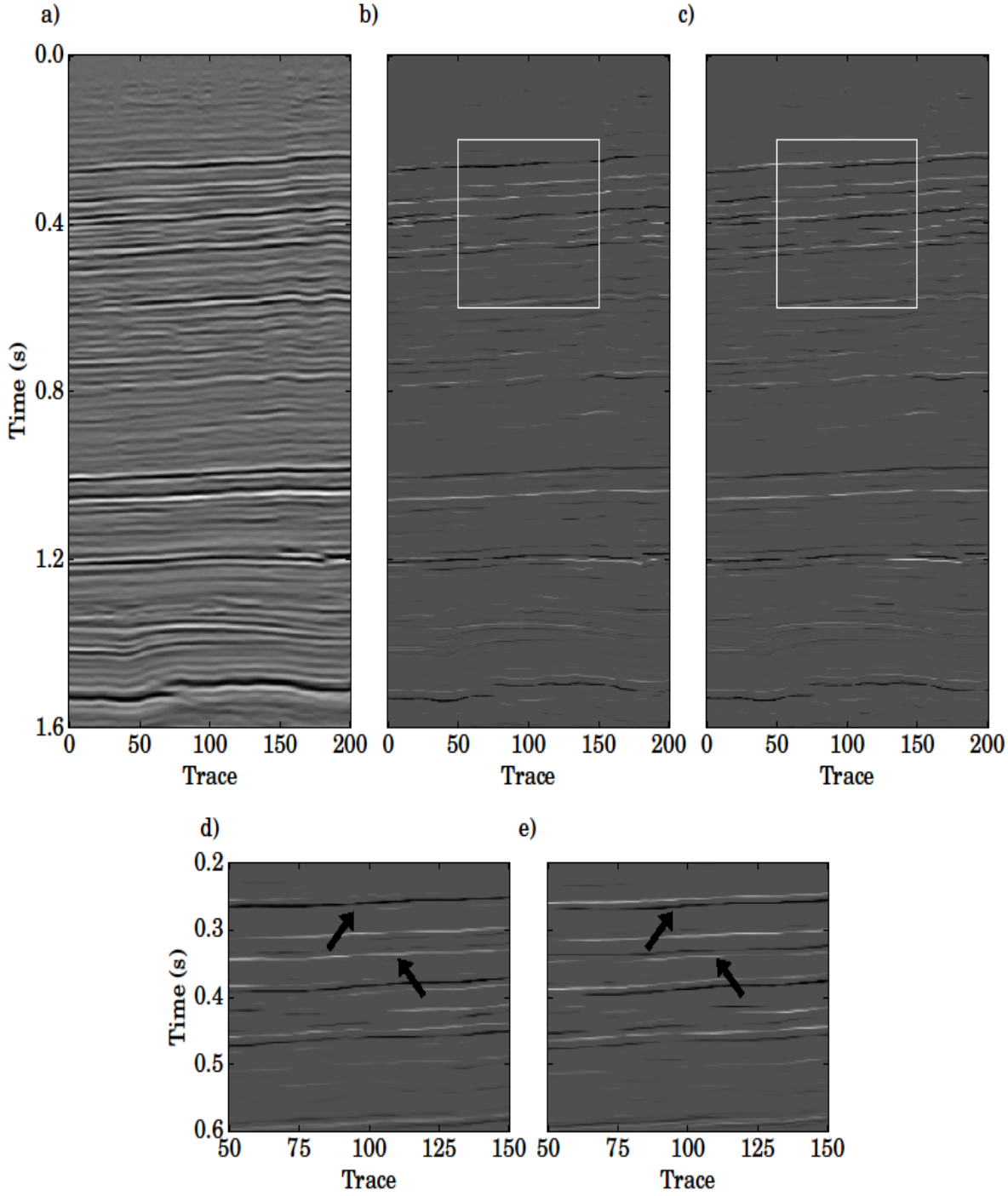

Fig. 8. Field data example: (a) Seismic section; (b) and (c) sparse-spike deconvolved sections using the wavelets estimated by means of the l_1-norm and the Kurtosis-based approaches, respectively; (e) and (d) regions indicated by the white rectangles in (b) and (c). The black arrows show the main differences between the two solutions.

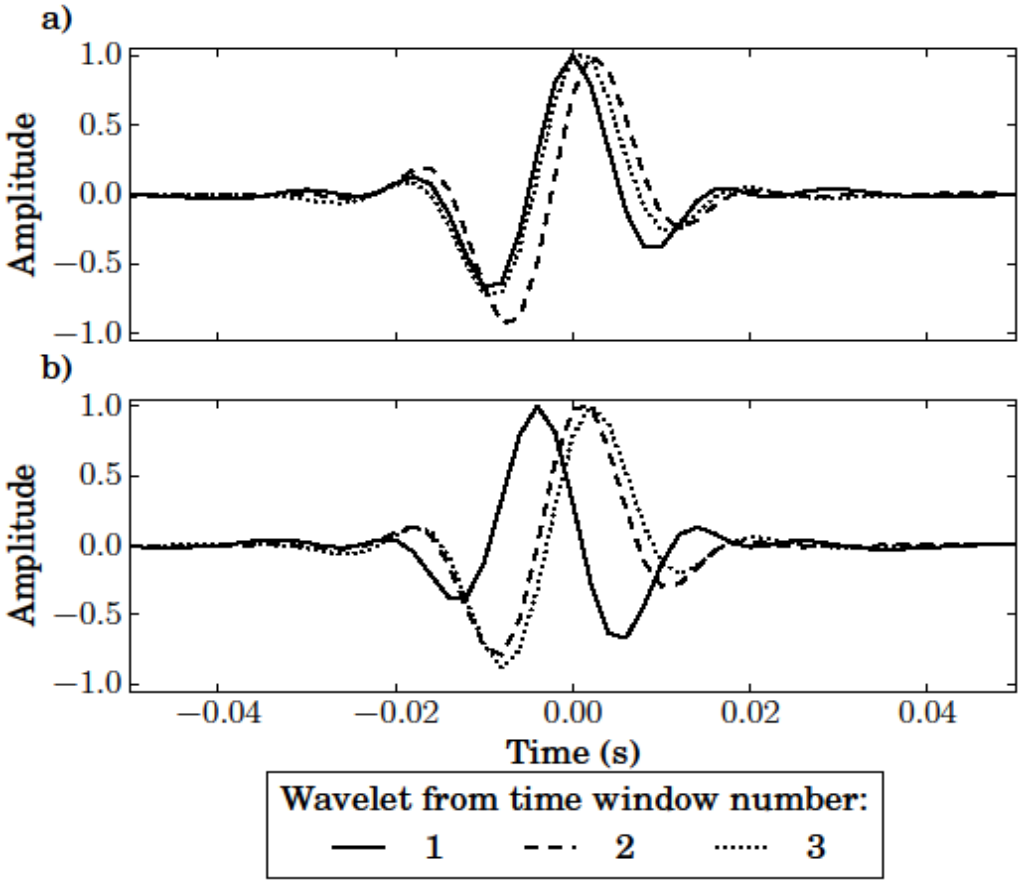

Fig. 9. Field data example: wavelets estimated in each analysis window using (a) the l_1-norm method, and (b) the Kurtosis-based approach.

CONCLUSION

Well-logs are usually considered as a ground truth to obtain wavelet phase information. However this information is not always available in the area of study. The method we present in this work can unveil the phase of the seismic wavelet directly from seismic data without any additional information. It assumes a non-Gaussian reflectivity and a constant phase. The optimum phase can be easily estimated by searching for the sparse-spike deconvolved trace whose l_1-norm is minimum. We showed that the phase estimates are rather inaccurate when the non-Gaussian hypothesis is not sufficiently fulfilled (Fig. 3). Even though, the proposed method provided usefull estimates for rather non-sparse reflectivities. We tested the proposed approach on synthetic 1D and 2D data under various S/N ratios, wavelet bandwidths and degrees of reflectivity sparseness. In all cases the proposed method showed more consistent and accurate estimates than those obtained using the classical Kurtosis-based technique. Contrarily, the Kurtosis-based

approach was more robust to noise, but yielded biased estimates that rapidly deteriorate with decreasing bandwidth and sparseness. Finally, we illustrated the new approach using field data and overlapping windows to take care of the wavelet non-stationarity. We showed that the phase estimates derived by means of the l_1-norm method led to more sparse and well-defined reflectivities than those obtained by means of the classical Kurtosis-based approach.

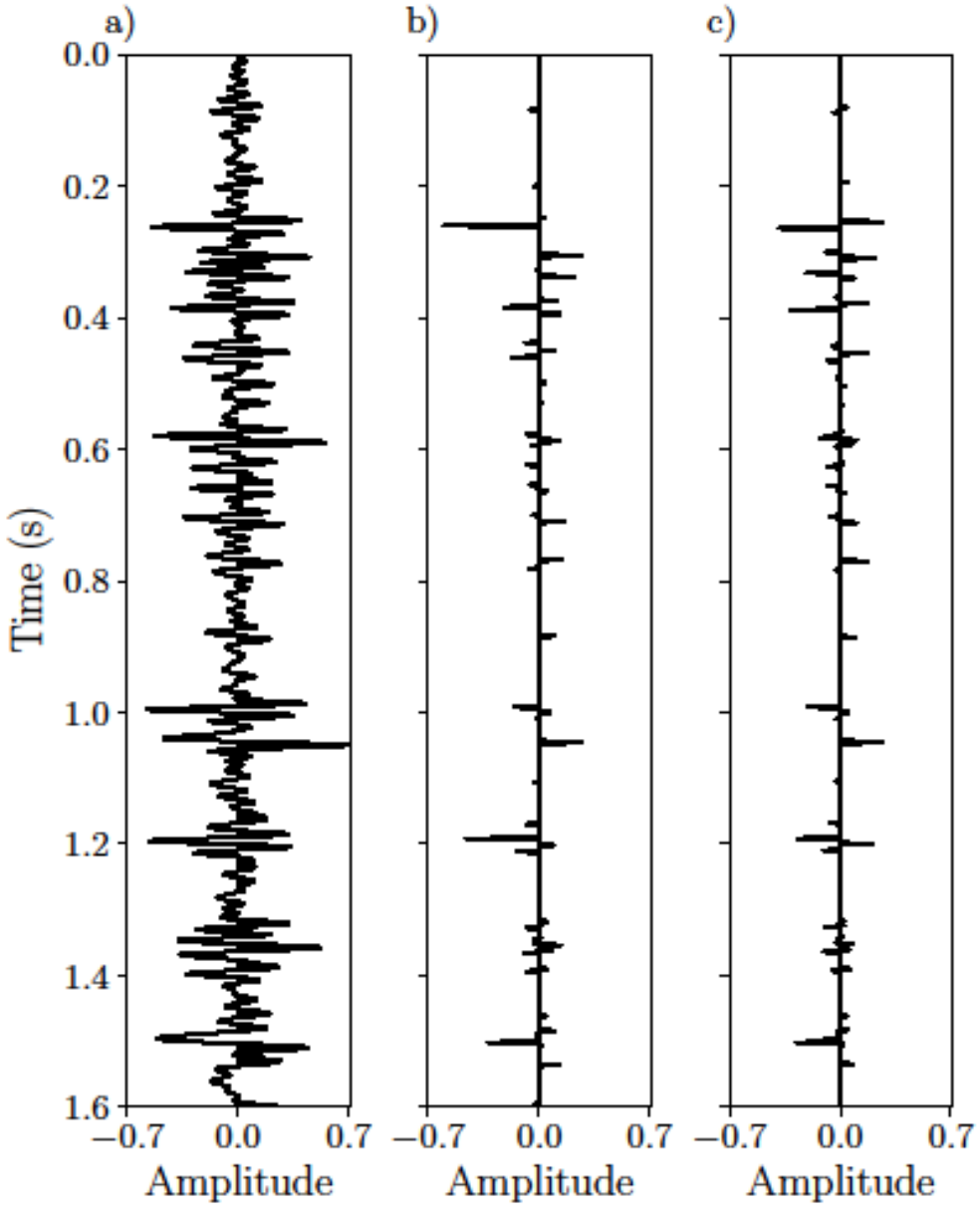

Fig. 10. Field data example: (a) trace number 100; (b) and (c) sparse-spike deconvolutions using the wavelets estimated by means of the l_1-norm and the Kurtosis-based approaches, respectively.

REFERENCES

Beaton, A., and Turkey, J., 1974. The fitting of power series, meaning polynomials, illustrated on band-spectroscopic data. Technometrics, 16: 147-185.

Beck, A., and Teboulle, M., 2009. A fast iterative shrinkage-thresholding algorithm for linear inverse problems. SIAM J. Imag. Sci., 2: 183-202.

Bioucas-Dias, J.M. and Figueiredo, M.A.T., 2007, A new twist: Two-step iterative shrinkage/thresholding algorithms for image restoration: IEEE Transact. Image Process., 16: 2992-3004.

Daubechies, I., Defrise, M. and Mol, C.D., 2004. An iterative thresholding algorithm for linear inverse problems with a sparsity constraint. Commun. Pure Appl. Mathemat., 57: 14131457.

Edgar, J., and van der Baan, M., 2011. How reliable is statistical wavelet estimation? Geophysics, 76: V59–V68.

Farquharson, C.G. and Oldenburg, D.W., 2004. A comparison of automatic techniques for estimating the regularization parameter in non-linear inverse problems. Geophys. J. Internat., 156: 411-425.

Figueiredo, M.A.T., Nowak, R.D. and Wright, S.J., 2007. Gradient projection for sparse reconstruction: Application to compressed sensing and other inverse problems. IEEE J. select. Top. Sign. Process., 1: 586-597.

Gramfort, A., Strohmeier, D., Haueisen, J., Hmlinen, M. and Kowalski, M., 2013. Time-frequency mixed-norm estimates: Sparse M/EEG imaging with non-stationary source activations. NeuroImage, 70: 410-422.

Hennenfent, G., van den Berg, E., Friedlander, M.P. and Hermann, F.J., 2008. New insights into one-norm solvers from the Pareto curve. Geophysics, 73: 23-26.

Herron, D., 2011. First Steps in Seismic Interpretation. SEG, Tulsa, OK.

Lazear, G., 1993. Mixed-phase wavelet estimation using fourth-order cumulants. Geophysics, 58: 1042-1051.

Levy, S. and Oldenburg, D.W., 1987. Automatic phase correction of common-midpoints stacked data. Geophysics, 52: P51-P59.

Longbottom, J., Walden, A.T. and White, R.E., 1988. Principles and application of maximum Kurtosis phase estimation. Geophys. Prosp., 36: 115-138.

Lu, W., 2005. Non-minimum-phase wavelet estimation using second and third-order moments. Geophys. Prosp., 53: 149-158.

Ma, M., Wang, S., Yuan, S., Wang, J., Wang, T., Haueisen, J., Hmlinen, M. and Kowalski, M., 2015. The comparison of skewness and Kurtosis criteria for wavelet phase estimation. Expanded Abstr., 85th Ann. Internat. SEG Mtg., New Orleans: 5164-5168.

Malinverno, A. and Briggs, V.A., 2004. Expanded uncertainty quantification in inverse problems: Hierarchical bayes and empirical bayes. Geophysics, 69: 1005-1016.

Martin, G.S., Wiley, R. and Marfurt, K.J., 2006. Marmousi2: An elastic upgrade for Marmousi. The Leading Edge, 25: 156-166.

Neidell, N., 1991. Could the processed seismic wavelet be simpler than we think? Geophysics, 56: P681-P690.

Oldenburg, D.W., Scheuer, T. and Levy, S., 1983. Recovery of the acoustic impedance from reflection seismograms. Geophysics, 48: 1318-1337.

Pérez, D.O., Velis, D.R. and Sacchi, M.D., 2013. High-resolution prestack seismic inversion using a hybrid FISTA least-squares strategy. Geophysics, 78: R185-R195.

Pérez, D.O., Velis, D.R. and Sacchi, M.D., 2017. Three-term inversion of prestack seismic data using a weighted $l_{2,1}$ mixed norm. Geophys. Prosp., 65, 1477-1495.

Robinson, E.A. and Treitel, S., 2002. Geophysical Signal Analysis. SEG, Tulsa, OK.

Sacchi, M.D., 1997. Reweighting strategies in seismic deconvolution. Geophys. J. Internat., 129: 651-656.

Taylor, H.L., Banks, S.C. and McCoy, J.F., 1979. Deconvolution with the l_1 norm: Geophysics, 44: 39-52.

Tugnait, J., 1987. Identification of linear stochastic systems via second- and fourth-order cumulant matching. IEEE Trans. Info. Theory, IT-33: 393-407.

van den Berg, E. and Friedlander, M., 2008. Probing the Pareto frontier for basis pursuit solutions. SIAM J. Sci. Comput., 31: 890-912.

van der Bann, M., 2008. Time-varying wavelet estimation and deconvolution by Kurtosis maximization. Geophysics, 73: V11-V18.

van der Bann, M. and Fomel, S., 2009. Nonstationary phase estimation using regularized local Kurtosis maximization. Geophysics, 73: A75-A80.

Velis, D.R., 2003. Estimating the distribution of primary reflection coefficients. Geophysics, 68: 1417-1422.

Velis, D.R., 2008. Stochastic sparse-spike deconvolution. Geophysics, 73, R1–R9.

Velis, D.R. and Ulrych, T.J., 1996. Simulated annealing wavelet estimation via fourth-order cumulant matching. Geophysics, 61: 1939-1948.

Walden, A. and Hosken, J., 1986. The nature of the non-Gaussianity of primary reflection coefficients and its significance for deconvolution. Geophys. Prosp., 34: 1038-1066.

Wang, Z., Zhang, B. and Gao, J., 2014. The residual phase estimation of a seismic wavelet using a Rényi divergence-based criterion. J. Appl. Geophys., 11: 96-105.

White, R., 1988. Maximum Kurtosis phase correction. Geophys. J. Internat., 95: 371-389.

Xu, Y., Thore, P. and Duchenne, S., 2012. The reliability of the Kurtosis-based wavelet estimation. Expanded Abstr., 82nd Ann. Internat. SEG Mtg., Las Vegas.

Yilmaz, O., 2001. Seismic Data Analysis: Processing, Inversion, and Interpretation of Seismic Data. Investigations in Geophysics, SEG, Tulsa, OK.

Yuan, S.Y. and Wang, X., 2011. Influence of inaccurate wavelet phase estimation on seismic inversion. Appl. Geophys., 8: 48-59.